Developing Fatigue Vehicle Models for Bridge Fatigue Assessment under Different Traffic Conditions

Lu Deng, Ph.D., M.ASCE[1]; Lei Nie[2]; Wenjie Zhong[3]; and Wei Wang, Ph.D.[4]

Abstract: The fatigue damage of steel bridges induced by heavy traffic loads is a critical problem worldwide. A uniform fatigue vehicle is generally adopted in bridge design codes to evaluate the cumulative fatigue damage of steel bridges. However, since the traffic loads vary across sites, a single vehicle with predetermined parameters may be imprecise for actual fatigue damage estimations. In this study, a new method for developing fatigue vehicle models that are applicable to various traffic conditions is proposed. The traffic in China was taken as an example for illustrating the proposed method. Numerical simulations were performed to investigate the fatigue damage distribution at 12 typical weigh-in-motion sites in China based on the collected vehicle load spectra, and the errors in fatigue damage estimations when adopting the fatigue vehicle Model III in Chinese bridge code were evaluated under various scenarios. Results showed that using Model III for fatigue analysis may seriously underestimate or overestimate the cumulative fatigue damage caused by the actual traffic loads under some conditions. Using a modified Model III with gross weight adjusted to the site-specific traffic condition could lead to a significant improvement, but the errors are still within a relatively large range. Following the classification and mathematical optimization techniques of the proposed method, a three-axle fatigue vehicle model and a four-axle fatigue vehicle model corresponding to the light and heavy traffic, respectively, were developed. These two fatigue vehicle models were proven to produce better and more consistent accuracy than the single fatigue vehicle model (i.e., Model III) for various traffic compositions in China. **DOI: 10.1061/(ASCE)BE.1943-5592.0001675.**

Author keywords: Highway bridge; Fatigue vehicle model; Traffic load spectrum; Genetic algorithm; Error analysis.

Introduction

With the rapid development of bridges, fatigue damage of steel bridges is prone to occur under a large amount of heavy traffic and can lead to serious disasters (Deng et al. 2017; Han et al. 2020; Qin and Gao 2017; Zhou and Zhang 2019). Accurate bridge fatigue assessment can give support for the maintenance of bridges that have suffered from traffic loads for many years and thus plays an essential role in bridge safety. Since the actual traffic loads on bridges are complicated and difficult to obtain, fatigue load models are generally used to represent the actual traffic loads in fatigue analysis (Croce 2001; Sedlacek et al. 2008). For example, a single fatigue vehicle has been widely used in a variety of fatigue analyses due to its simplicity (Deng and Yan 2018). Actually, fatigue vehicle models have been documented in bridge specifications of many countries or regions, e.g., the fatigue truck in AASHTO of the United States, the Fatigue Load Model 3 in Eurocode 1 of the European Union, and the fatigue load calculation Model III in JTG D60-2015 and JTG D64-2015 of China (AASHTO 2017; CEN 2003; JTG D60-2015, GB 2015a; JTG D64-2015, GB 2015b). It is worth mentioning that, according to the clause explanation of Chinese *Specifications for Design of Highway Steel Bridge* JTG D64-2015, Model III in the Chinese bridge specification was developed based on the Eurocode EN 1991-2 Fatigue Load Model 3 (FLM3) by just modifying the ground contact dimensions of wheels. The traffic data used to build FLM3 were obtained from two survey activities conducted in Europe between 1977–1982 and 1984–1988 (Sedlacek et al. 2008). Therefore, it may not be suitable to use Model III to estimate the bridge fatigue damage caused by traffic load in China.

One of the main goals of studying fatigue load models is to develop single fatigue vehicles that can produce the same fatigue damage as the actual traffic load in the calculation (Chen et al. 2015; Laman and Nowak 1996). Some researchers and engineers focused on establishing fatigue load models applicable to different regions. Laman and Nowak (1996) proposed a three-axle and a four-axle fatigue vehicle based on the traffic load investigations of five steel bridges in the United States. The three-axle and four-axle fatigue vehicles are applicable to calculate the fatigue damage of bridges induced by vehicles with 2–9 and 10–11 axles, respectively. They also observed very large errors in the cumulative fatigue damage when using the fatigue truck model in the AASHTO code, especially for short-span bridges.

While a single fatigue vehicle model with determined parameters can be very convenient for application, it is generally believed that it is more accurate to utilize the collected actual traffic load data than using a single fatigue vehicle model in the fatigue analysis (Ma et al. 2018). In fact, Laman and Nowak (1996) also pointed out that an accurate fatigue vehicle model is strongly site-specific and characterized by the local truckload spectrum. Much effort has been devoted to proposing fatigue vehicles based on the weigh-in-motion (WIM) data of a certain region, e.g., a specific

[1]Professor, Hunan Provincial Key Laboratory for Damage Diagnosis for Engineering Structures, Hunan Univ., Changsha 410082, Hunan, China. Email: denglu@hnu.edu.cn

[2]Graduate Student, College of Civil Engineering, Hunan Univ., Changsha 410082, Hunan, China. Email: nielei@hnu.edu.cn

[3]Graduate Student, College of Civil Engineering, Hunan Univ., Changsha 410082, Hunan, China. Email: wjzhong@hnu.edu.cn

[4]Assistant Professor, Hunan Provincial Key Laboratory for Damage Diagnosis for Engineering Structures, Hunan Univ., Changsha 410082, Hunan, China (corresponding author). Email: wei_wang@hnu.edu.cn

Note. This manuscript was submitted on January 15, 2020; approved on September 22, 2020; published online on December 7, 2020. Discussion period open until May 7, 2021; separate discussions must be submitted for individual papers. This paper is part of the ***Journal of Bridge Engineering***, © ASCE, ISSN 1084-0702.

province in China (Chen et al. 2015) and a specific state in the United States (Chotickai and Bowman 2006), or even a bridge in a certain city (Ma et al. 2018). The application of these fatigue vehicles is limited to regions where the traffic data are collected from and the models may not produce satisfactory accuracy when used to calculate the fatigue damage of bridges under the traffic loads of other regions. It is noted that fatigue vehicle models are usually intended for sites where the traffic load level is relatively high. Therefore, using these models for sites where the traffic load level is relatively low may result in excessive overestimation of fatigue damage (Chen et al. 2015; Zhou et al. 2010).

In China, plenty of research on fatigue vehicle models based on monitored traffic load data has been carried out. For example, Tong et al. (1997) proposed a vehicle load spectrum using the collected traffic data of a bridge at Shanghai's inner ring, which is the first study on the fatigue load spectrum in China. Zhou et al. (2010) conducted on-site traffic load surveys at eight typical highway and bridge toll stations in China and developed separate fatigue vehicles for different regions. The fatigue vehicle for Liaoning Province in Zhou et al. (2010) was adopted as the standard fatigue vehicle in China. A single-vehicle fatigue load model based on the WIM traffic data at three typical sites in Guangdong Province was given in Chen et al. (2015), and the model was believed to be applicable to heavily loaded areas of China since the load levels in Guangdong were higher than those of other regions (Yan et al. 2012). Liu et al. (2017b) investigated the vehicle load distributions in 23 provinces of China in detail and suggested a three-axle, a four-axle, and a six-axle fatigue vehicle model for Zhejiang, Guizhou, and most other provinces of China, respectively. Ma et al. (2018) developed seven fatigue vehicles for the fatigue assessment of the steel box-girders of XiHouMen Bridge based on the on-site-collected WIM data.

Till now, a few studies on high-accuracy fatigue vehicle models that are suitable for various sites where the traffic load compositions are different have been conducted. In this paper, a new method is proposed for determining fatigue vehicle models that can be applied to fatigue damage calculations at various sites where the traffic load compositions are different. Using the collected vehicle load spectra at 12 typical sites in China as an example, a three-axle fatigue vehicle model and a four-axle fatigue vehicle model are suggested for the light-duty and heavy-duty traffic, respectively. These two fatigue vehicle models have proven better and more consistent accuracy than the current fatigue vehicle model in the Chinese code. Therefore, they can not only be used directly as a reference for bridge fatigue evaluation in China but also serve as examples for developing fatigue vehicle models with improved accuracy in other regions.

Collected Fatigue Load Spectra

Accurate fatigue damage analysis of bridges should be based on the actual traffic load data. However, due to the diversity and complexity of actual traffic loads, direct use of the original traffic load data may cause inconvenience in the fatigue analysis process. To cope up with the problem, fatigue load spectra are widely utilized in the vehicle-induced fatigue analysis (Chen et al. 2015; Liu et al. 2017b; Zhou et al. 2009).

Since China covers a very large geographic area and the traffic condition in China varies significantly between different areas, the traffic in China was selected as the background for the fatigue evaluation of bridges and for developing fatigue vehicle models in this study. Fatigue load spectra at 12 typical sites in China were selected as the sources of the traffic data. These sites are located in 12 different provinces or municipalities in China, namely, Beijing, Fujian, Guangdong, Henan, Jiangsu, Jiangxi, Liaoning, Shandong, Shanghai, Shanxi, Sichuan, and Zhejiang. For the convenience of description, these sites were numbered from RD1 to RD12 in the order of the provinces in which they are located. These data are representative of Chinese actual traffic loads because the selected provinces or municipalities are distributed in different regions throughout China. For example, Liaoning is located in the northeast region, Beijing and Shanxi belong to the northern region, Henan is in the central region, Sichuan is located in the southwest region, Jiangsu and Fujian are in the eastern coastal region, and Guangdong is in the southern region. The traffic in the northwestern region of China was excluded in this study due to the underdeveloped traffic in the region and the lack of traffic statistics. All traffic load spectra were collected from existing references (Liu et al. 2014a, 2017a; Liu 2017; Shao and Lu 2015; Su et al. 2018; Sun and Sun 2012; Tong et al. 1997; Yang 2015; Yin 2016; Zhao 2014; Zhou et al. 2009, 2010). These load spectra were collected based on traffic investigation of more than 6.23 million trucks in total by multiple research teams during the period of 1995–2017. These traffic loads were collected in a variety of ways, including the bending plate WIM system on urban loop expressways, the weighing system used on toll stations of freeways and bridges, and on-site manual measurements. It should be noted that vehicles with a gross weight below 30 kN were omitted in the traffic statistics and fatigue analysis procedures because these vehicles have very limited contribution to the fatigue damage (Lu et al. 2017; Zhou et al. 2010). Table 1 exhibits the fatigue load spectrum of RD10 in Shanxi Province provided in Zhou et al. (2010). The fatigue load spectra of other sites are not exhibited due to space restrictions.

Laman and Nowak (1996), Raju et al. (1990), and Schilling (1984) suggested that the axle weights of a fatigue vehicle should be adjusted in proportion to the equivalent gross vehicle weight (EGVW) if the load distribution data at the specific site are available to improve the accuracy of the fatigue evaluation results, and the EGVW can be calculated by the following equation:

$$\mathrm{EGVW} = \left(\sum_i f_i \mathrm{GVW}_i^3 \right)^{1/3} \tag{1}$$

where f_i = frequency of occurrence of the ith vehicle in the load spectrum; and GVW_i = gross vehicle weight of the ith vehicle in the load spectrum. The EGVW values at different sites are shown in Table 2. These EGVW values were used to illustrate the effectiveness of the strategy of adopting the site-specific EGVW in the fatigue analysis.

Table 1. Fatigue load spectrum at RD10 in Shanxi Province

Number of axles	Axle weight (kN)	Axle spacing (m)	Gross weight (kN)	Relative frequency (%)
2	40, 100	4.0	140	29.4
3	50, 75, 150	2.8, 3.5	275	3.8
4	55, 65, 140, 140	2.0, 4.5, 1.4	400	7.6
5	50, 140, 100, 100, 100	3.5, 6.2, 1.8, 1.4	490	11.1
6	50, 105, 130, 110, 110, 110	2.6, 2.0, 7.0, 1.4, 1.4	615	48.2

From Table 2, it can be found that the EGVW at different sites presented a very large variation. The minimum value of EGVW in the selected sites was 180 kN at RD9 in Shanghai, while the maximum value was 508 kN at RD10 in Shanxi.

In the United States, the Federal Highway Administration (FHWA) divides vehicles into 13 classes, and the Federal Bridge Formula B is widely utilized to limit vehicle weights. Bridge Formula B takes the distance between the outermost two axles of an axle group and the number of axles in that axles group as parameters to calculate the allowable weight limit of a group of axles. In addition, Bridge Formula B sets an upper limit of 36.3 tons for the gross weight of all vehicles. Differently, the Chinese national standard GB1589-2016 divides axles into single axle, two-axle group, and three-axle group and limits the axle weight based on the characteristics of each axle/axle group in the form of a table. In addition, GB1589-2016 divides all vehicles into 19 vehicle types and imposes a total weight limit on each vehicle type. It should be emphasized that GB1589-2016 sets the upper limit of the gross vehicle weight to 49 tons, which is much higher than the upper limit of 36.3 tons allowed by Bridge Formula B. Due to the differences in vehicle types, axle limits, and other factors in different countries or regions, the actual traffic load in different regions varies greatly. Therefore, it is necessary to propose suitable fatigue load models for different regions based on regional traffic characteristics.

Fatigue Damage Calculation Method

According to the "General Design Atlas of the Superstructure of Highway Bridge Structures," which is widely used by Chinese bridge designers, simply supported girder bridges with a span length of 6–40 m and continuous girder bridges with a single span length of 16–40 m are the two main bridge types for medium and small bridges in China. Therefore, in the present study, simply supported girder bridges with spans of 6–40 m and continuous girder bridges with two equal spans of 16–40 m were selected. According to Brühwiler and Herwig (2008) and González et al. (2011), the bending moment generally governs the requirements of bridge sections. Thus, only bending stresses on girders were calculated. The fatigue damage at three critical sections, namely, the midspan of the simply supported girder bridges and the midspan and midsupport of the two equal-span continuous girder bridges, was considered, and these three damage locations were marked as DL1, DL2, and DL3, respectively. The damage locations and their corresponding moment influence lines are shown in Fig. 1.

Miner's hypothesis, which is suggested by the AASHTO LRFD code, was adopted for cumulative fatigue damage calculations (AASHTO 2017; Miner 1945). Since Miner's hypothesis assumes that the material fatigue damage is linearly accumulated under repeated loads, the cumulative fatigue damage (D) could be expressed as the sum of damage caused by every single cycle. Due to the fact that the vehicle-load-induced stress cycles are complex and cannot be directly applied to fatigue damage calculations, the rainflow-counting method was utilized to decompose the original stress cycles into a primary stress range and higher-order stress ranges (Downing and Socie 1982). According to the research in Schilling (1984), the single-vehicle-induced cumulative fatigue damage (D) could be expressed by the primary stressed range ($S_{r,\max}$) with the corresponding equivalent number of stress cycles (N_e):

$$D = \frac{N_e S_{r,\max}^3}{C} \tag{2}$$

$$N_e = 1 + \left(\frac{S_{r,1}}{S_{r,\max}}\right)^m + \left(\frac{S_{r,2}}{S_{r,\max}}\right)^m + \cdots + \left(\frac{S_{r,i}}{S_{r,\max}}\right)^m \tag{3}$$

where $S_{r,\max}$ = primary or maximum stress range in the cycle; $S_{r,i}$ = higher-order stress range; m = slope constant of the S–N curve of the fatigue detail, which equals approximately 3 for all kinds of fatigue category details in AASHTO (Schilling and Klippstein 1977); and C = parameter related to the fatigue category detail.

Table 2. EGVW values at 12 sites

Site	EGVW (kN)
RD1	223.2
RD2	272.5
RD3	442.8
RD4	430.3
RD5	344.5
RD6	357.3
RD7	439.6
RD8	355.6
RD9	180.8
RD10	508.6
RD11	212.6
RD12	237.9

Analysis of Traffic Loads in China

Vehicle Type Composition

The vehicle type proportions (by the number of axles) at 12 sites obtained by the analysis of the collected traffic load spectra are plotted in Fig. 2.

It is observed in Fig. 2 that the proportion of each vehicle type varied greatly from site to site. For example, a six-axle vehicle was the main vehicle type at RD3, RD4, and RD10, accounting for more than 40% of the total number of vehicles. In contrast, over 70% of the total vehicles at RD11 and RD12 are two-axle vehicles and the six-axle vehicle took up less than 10%.

In addition, as shown in Fig. 2 and Table 2, the two-axle vehicle occupied more than 50% of the total number of vehicles at RD11 and RD12, and the EGVW values at these two sites were relatively

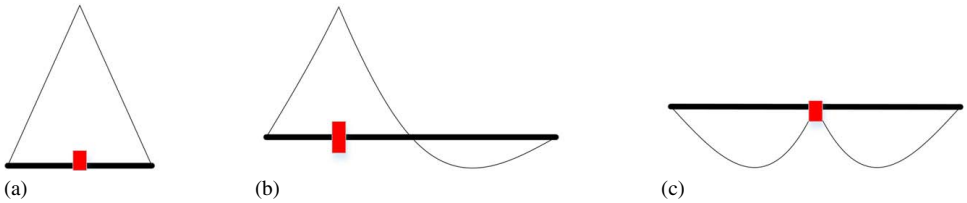

Fig. 1. Three damage locations (rectangular blocks) and the corresponding moment influence lines: (a) midspan of the simply supported bridge (DL1); (b) midspan of the continuous bridge (DL2); and (c) midsupport of the continuous bridge (DL3).

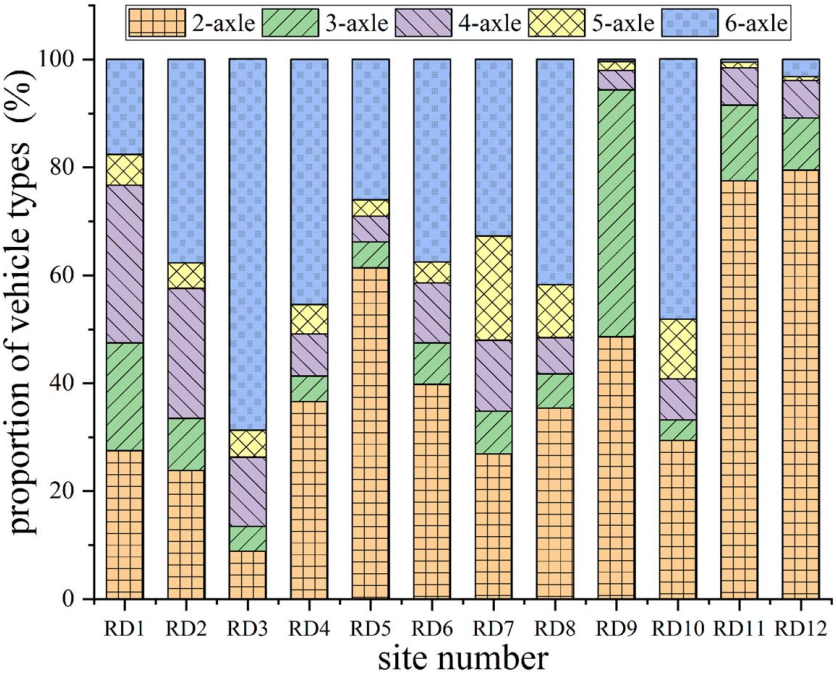

Fig. 2. Proportion of each vehicle type (by the number of axles).

low. In contrast, the six-axle vehicle was the most numerous of all vehicle types at RD3, RD4, RD7, and RD10, and the EGVW values at these sites were relatively high. It can be concluded that the EGVW was highly related to the proportion of each vehicle type. The larger the value of EGVW, the larger the proportion of six-axle vehicles and the smaller the proportion of two-axle vehicles.

Damage Composition

The damage contribution ratio (DCR), which represents the proportion of the fatigue damage caused by each vehicle type, was calculated at each site to analyze the damage distribution. The moment time history at each damage location caused by the passage of each vehicle in the load spectrum was calculated by using the moment influence lines (Fig. 1) and the axle weights and spacings of vehicles in the load spectrum. Then, the primary moment range and the equivalent number of cycles caused by the passage of each vehicle in the load spectrum were computed by using the rain-flow counting method and Eq. (3). Finally, the DCR value of the ith vehicle in the load spectrum was calculated by Eq. (4). It should be noticed that the stresses at the fatigue damage points were assumed to be proportional to the bending moments of the sections; thus, the ratio of two stress ranges would be equal to the ratio of the corresponding moments:

$$\mathrm{DCR}_i = \frac{f_i D_i}{\sum f_i D_i} = \frac{f_i N_{e,i} S_{r,\max,i}^3}{\sum f_i N_{e,i} S_{r,\max,i}^3} = \frac{f_i N_{e,i} M_{r,\max,i}^3}{\sum f_i N_{e,i} M_{r,\max,i}^3} \tag{4}$$

where D_i = fatigue damage caused by the passage of the ith vehicle in the load spectrum; $S_{r,\max,i}$, $M_{r,\max,i}$, and $N_{e,i}$ = primary stress range, the primary moment range, and the corresponding equivalent number of cycles caused by the passage of the ith vehicle in the load spectrum, respectively. Due to limitations on the paper length, the DCRs at RD10, RD11, and RD12 were selected as examples, as shown in Fig. 3. Besides, 6, 16, 25, and 40 m were selected as example single span lengths for illustration.

It can be found in Fig. 3 that the proportion of fatigue damage at different sites may vary greatly. For example, at RD10, the six-axle vehicle contributed over 60% of the total fatigue damage under all considered conditions, while other types of vehicles contributed very little. However, at RD11, the two-axle vehicle caused more fatigue damage than other types of vehicles, while the six-axle vehicle contributed very little. In addition, large differences might exist between the DCR and the corresponding quantitative proportion of each vehicle type. For example, at site RD12, the six-axle vehicle occupied only 3.2% of the number of vehicles in the traffic; however, it brought over 30% of the total fatigue damage, which was more than any other type of vehicle. Therefore, it can be concluded that heavy vehicles could also cause a large proportion of fatigue damage in the case of a small quantity proportion in some areas. In addition, the fatigue damage contribution changed irregularly with the damage locations and the span lengths of bridges.

Fatigue Evaluation Using Vehicle Model III

Two Chinese bridge specifications, namely, *Specifications for Design of Highway Steel Bridge* (JTG D64) and *General Specifications for Design of Highway Bridges and Culverts* (JTG D60), suggest the single-vehicle fatigue load model, namely, the fatigue load calculation Model III (Model III), for the fatigue damage estimation of bridge components directly bearing wheel loads (JTG D60-2015, GB 2015a; JTG D64-2015, GB 2015b). The axle weight and axle spacing configuration of the model are shown in Fig. 4.

As concluded previously, the quantity proportion of each vehicle type and fatigue damage distribution varied greatly from site to site. The accuracy of the model was verified at various sites based on monitored traffic load to examine the applicability of the fatigue load Model III under Chinese traffic circumstances. The fatigue damage ratio (FDR), which equals the ratio of the fatigue damage caused by the passage of the fatigue vehicle to that caused by the measured traffic load spectrum, was adopted to evaluate the accuracy of the fatigue load model. The calculation process of FDR is shown in Eq. (5). Assuming that the bridge conforms to

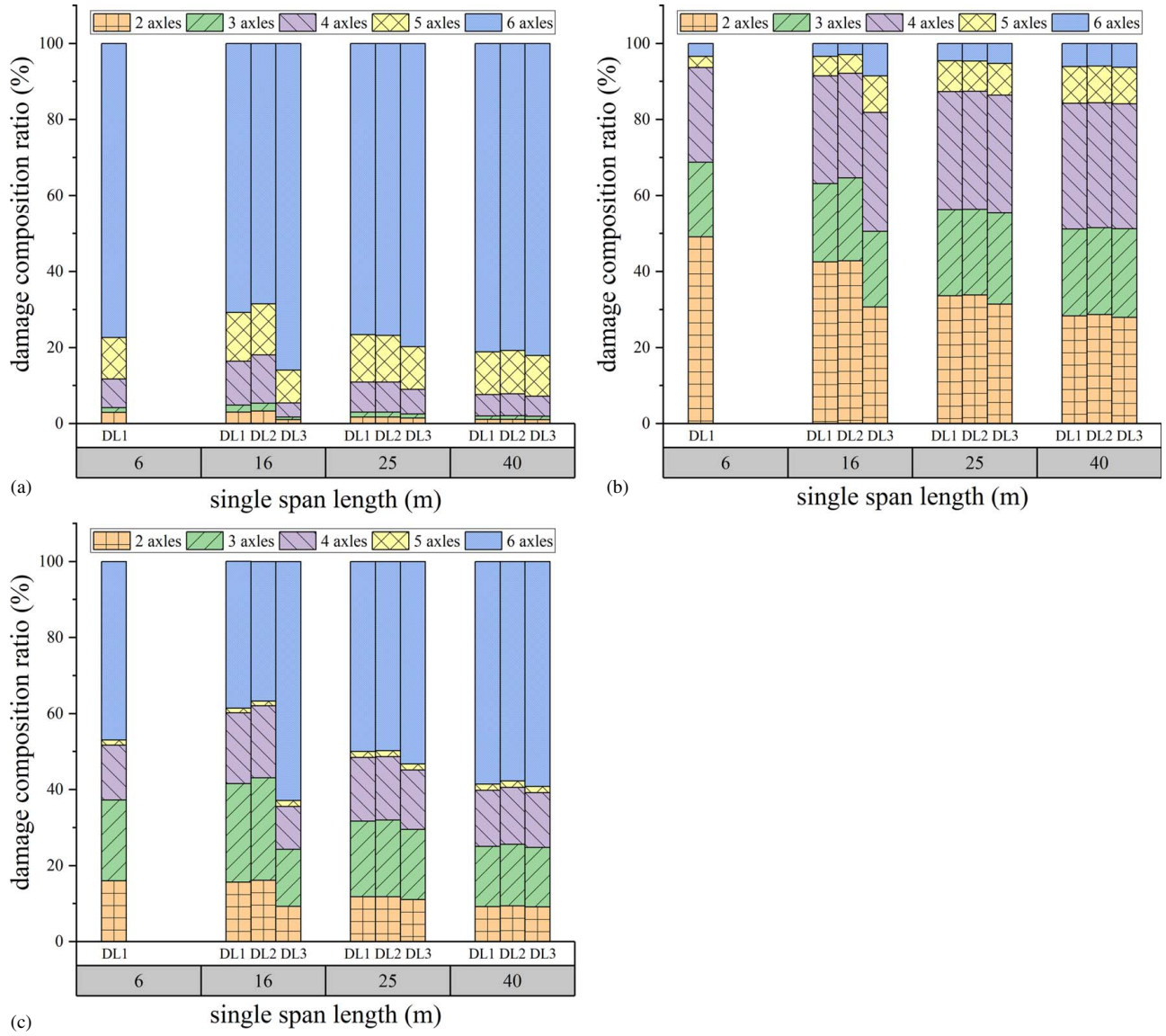

Fig. 3. Damage composition ratios (by the number of axles): (a) at RD10 (located in Shanxi); (b) at RD11 (located in Sichuan); and (c) at RD12 (located in Zhejiang).

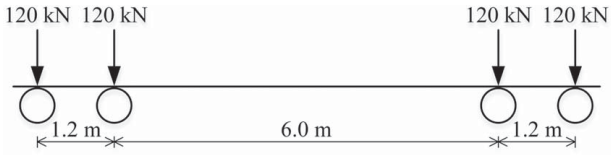

Fig. 4. Fatigue load calculation Model III in Chinese specification.

the flat section assumption and the materials are in the stage of linear elasticity, then

$$\mathrm{FDR}=\frac{D_{\mathrm{model}}}{D_{\mathrm{actual}}}=\frac{D_{\mathrm{model}}}{\sum f_i\cdot D_i}=\frac{\frac{S_{rm}^3N_{em}}{C}}{\sum f_i\frac{S_{r,\max,i}^3N_{e,i}}{C}}=\frac{\frac{M_{rm}^3y_D^3N_{em}}{I_z^3C}}{\sum f_i\frac{M_{r,\max,i}^3y_D^3N_{e,i}}{I_z^3C}}=\frac{M_{rm}^3N_{em}}{\sum f_iM_{r,\max,i}^3N_{e,i}} \quad (5)$$

where S_{rm}, M_{rm}, and N_{em} = primary stress range, the primary moment range, and the corresponding equivalent number of cycles caused by the passage of the fatigue vehicle, respectively; I_z = moment of inertia of the cross section; and y_D = distance from the fatigue point to the neutral axis. The FDR calculation process does not need to determine the classification of fatigue details and related parameters; the detail parameter C exists in both the numerator and the denominator and can be eliminated together.

The damage computed by the passage of ideal fatigue vehicles should be the same as that calculated using the measured load spectrum with an equal number of vehicle passages (Laman and Nowak 1996). Therefore, errors of the fatigue damage calculated by the fatigue vehicle can be well evaluated by the FDR. An FDR equal to 1 means that the fatigue damage calculated by the fatigue vehicle can accurately reflect the fatigue damage caused by the actual traffic load. Besides, an FDR greater than 1 means that the calculated result by the fatigue vehicle may overestimate the actual fatigue damage and vice versa. Based on the analysis, the FDRs at different sites are plotted in Fig. 5.

It can be found from Fig. 5 that the FDR values of Model III varied widely at different sites, which means that the relative errors of

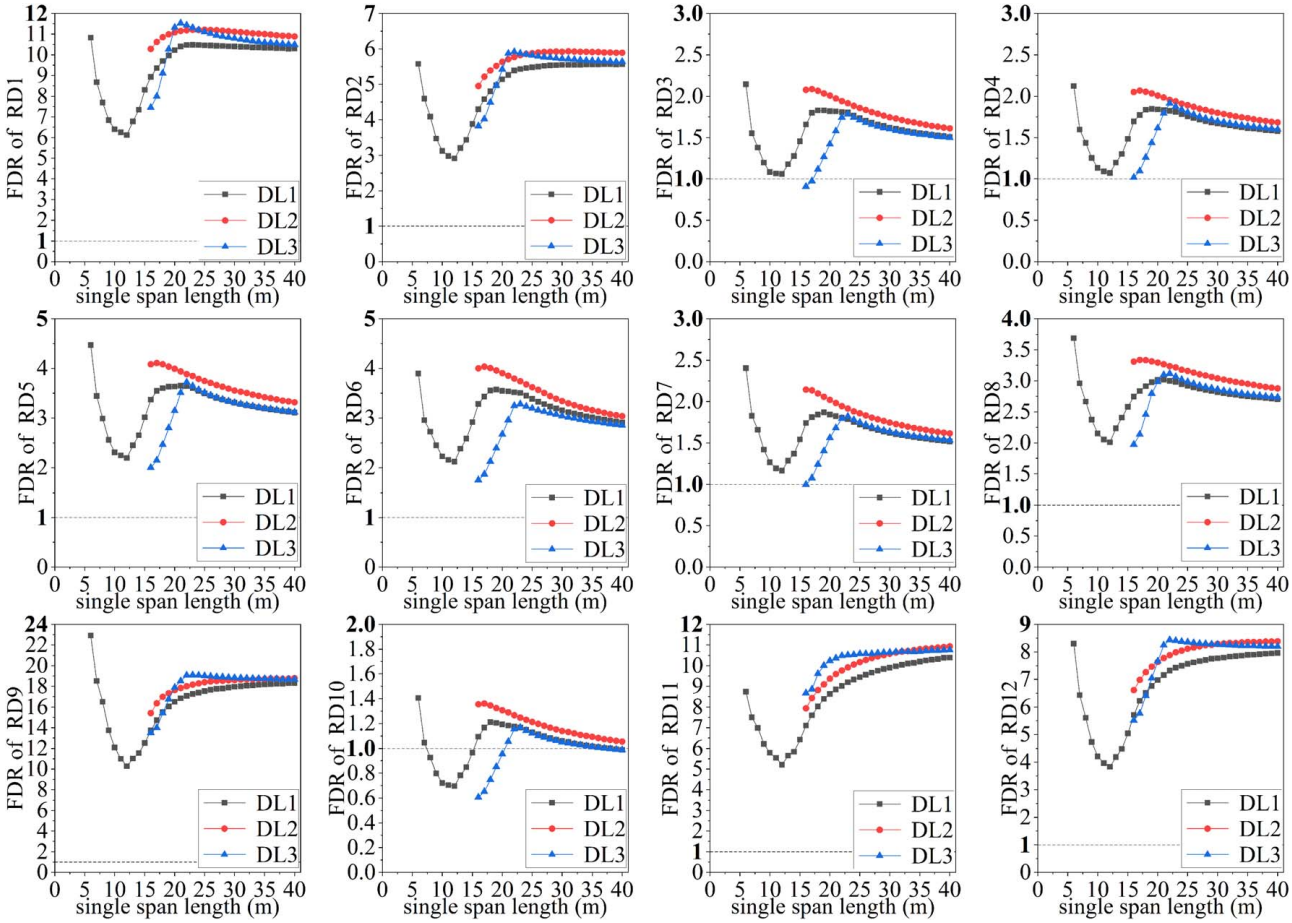

Fig. 5. FDR of Model III at 12 sites.

Model III are highly dependent on the traffic load composition. In addition, it is noted that for some short bridges in some area, the FDR value can reach 20, meaning that using Model III directly can significantly overestimate the vehicle-induced fatigue damage under certain circumstances.

Some researchers suggested that if the load distribution data at the specific site are available, the axle weights of a fatigue vehicle should be adjusted in proportion to the EGVW to improve the accuracy of the fatigue evaluation results. Following this strategy, the EGVW values as calculated in Table 2 are adopted to recalculate the fatigue damage, and the results are shown in Fig. 6.

As shown in Fig. 6, by adopting the site-specific EGVW values, the range of the calculated FDR values was reduced significantly. The newly calculated FDR values ranged from 0.46 to 1.84, meaning that using the adjusted Model III with site-specific EGVW (will be referred to as the adjusted Model III hereafter), can significantly improve the accuracy of fatigue damage evaluation.

In addition, it is found that when the span length of a simply supported bridge was smaller than 12 m, the FDR of the adjusted Model III at DL1 decreased as the span length increased. However, the FDR increased with increasing span length for bridges with the single-span length between 12 and 23 m. When the span length was greater than 23 m, the FDR at the three selected damage locations either increased or decreased to the ultimate value approaching unity. It can be concluded that the fatigue damage estimation accuracy of the adjusted Model III is still insufficient and fluctuates considerably for bridges shorter than 23 m, while the accuracy increases with increasing span length when the single-span length is larger than 23 m.

Besides, the relative errors of fatigue damage calculated by using the adjusted Model III for simply supported bridges with span lengths around 12 m are smaller than those of bridges with other spans. In some special cases, such as 12 m simply supported bridges at RD11 and RD12, the actual fatigue damage value may reach more than two times the calculated value. In these conditions, using the adjusted Model III for fatigue assessment may seriously underestimate the effects of actual fatigue damage.

In addition, the estimation errors of the adjusted Model III may exhibit large differences at different damage locations on the same bridge. For example, for a 2×16 m continuous bridge at RD7, the estimated fatigue damage by using the adjusted Model III is approximately 1.6 times the actual value at the midspan but is about 0.7 times the actual value at the midsupport. However, when the single-span length of the bridge is larger than 23 m, the relative errors at three damage locations are similar, which means that the error is not sensitive to the fatigue damage location for large-span bridges.

From the previous analysis, it can be concluded that due to the large diversity of traffic load composition, bridge span length, and damage location, the errors of the estimated fatigue damage by using Model III can be very large. By adopting the adjusted Model III with site-specific EGVW, the errors can be significantly reduced. However, due to the inherent limitation with the single fatigue vehicle model, namely, Model III, the errors were still within a relatively large range. Therefore, a new fatigue vehicle model

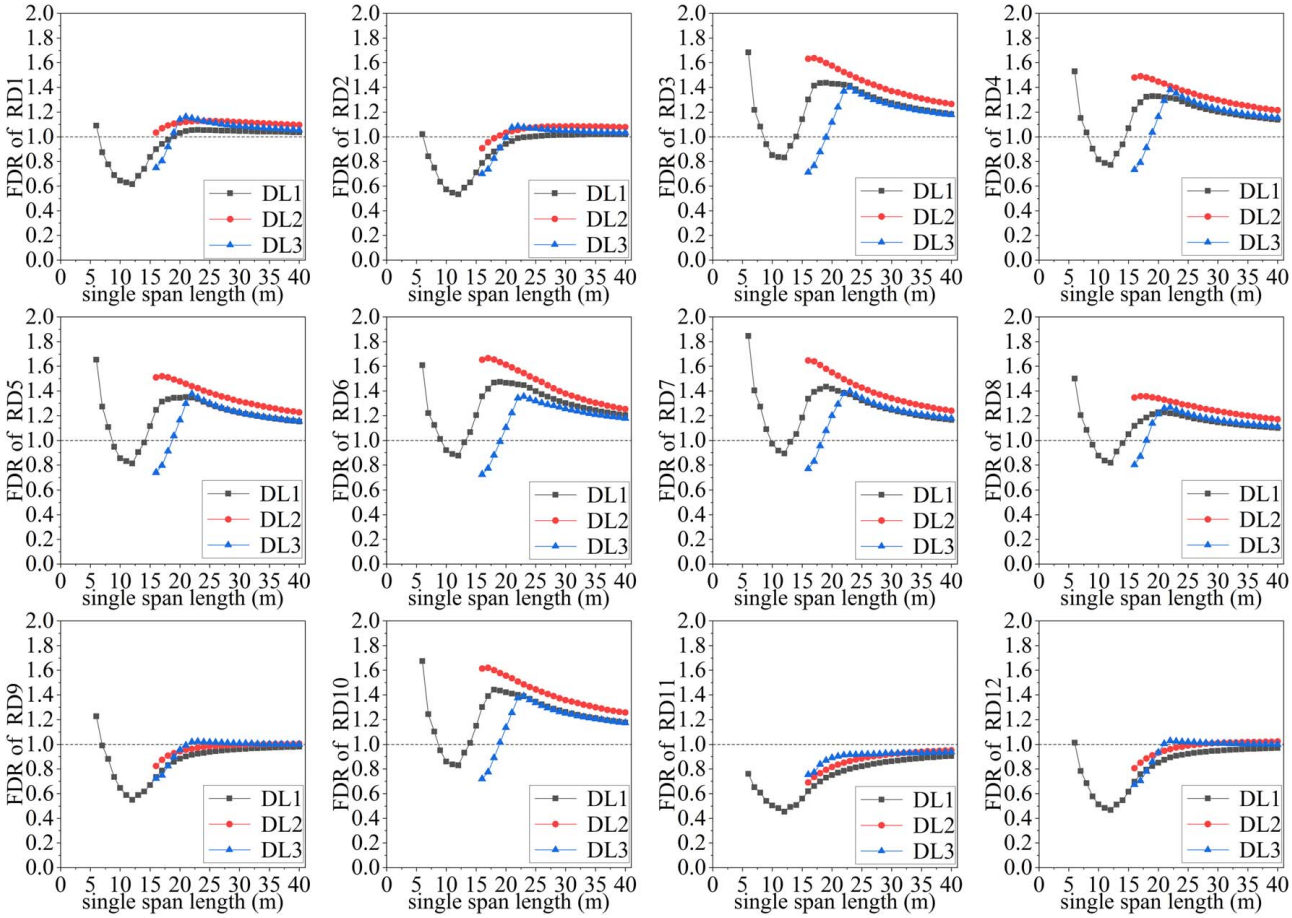

Fig. 6. FDR of the adjusted Model III at 12 sites.

needs to be proposed to improve the accuracy of the fatigue damage estimations under various traffic conditions in China.

Development of Fatigue Vehicle Models

Process of the Optimization Method

For regions that cover a large geographic area like China, due to the large difference in traffic load compositions at different sites, the diversity of bridge span lengths and damage locations, and the unclear relationship between different model parameters and fatigue damage calculation results, it is difficult to propose an accurate fatigue vehicle model that can be applied under various conditions by using regular methods.

A mathematical optimization method was utilized in this section to find a fatigue vehicle that was accurate under all selected conditions. The physical fatigue vehicle model is converted to a mathematical model with key variable parameters, namely, the number of axles, the axle weight ratio ($\boldsymbol{W}$), and the axle spacing ($\boldsymbol{L}$). The EGVW, which is calculated by the traffic load spectrum, is adopted in the fatigue damage calculation. Therefore, each actual axle weight of the fatigue vehicle can be calculated by the EGVW and the axle weight ratio ($\boldsymbol{W}$). A three-axle fatigue vehicle model or a four-axle fatigue vehicle model is commonly adopted as the fatigue vehicle models in bridge design specifications of different countries. For example, the European EN 1991-2 code, the British BS 5400 code, and the Chinese JTG D64-2015 code all adopt a four-axle fatigue vehicle model, while the AASHTO LRFD bridge design specification adopts a three-axle fatigue vehicle model. Therefore, the three-axle vehicle and the four-axle vehicle were both considered as the possible form of the fatigue vehicle. In addition, it is worth mentioning that although a three-axle fatigue vehicle model or a four-axle fatigue vehicle model may be a good choice, other vehicles with different configurations that can represent the fatigue damage induced by actual traffic loads may also satisfy the requirement. When the fatigue vehicle was assumed to be a three-axle vehicle, the variable parameters were set as shown in Eq. (6). When the fatigue vehicle was assumed to be a four-axle vehicle, the variable parameters were set as shown in Eq. (7).

$$\begin{aligned} \boldsymbol{W} &= \{w_1, w_2, w_3\} \\ \boldsymbol{L} &= \{l_1, l_2\} \end{aligned} \tag{6}$$

$$\begin{aligned} \boldsymbol{W} &= \{w_1, w_2, w_3, w_4\} \\ \boldsymbol{L} &= \{l_1, l_2, l_3\} \end{aligned} \tag{7}$$

where w_i = ratio of the ith axle weight to the gross vehicle weight; and l_i = spacing between the ith and $(i+1)$th axles. There were four independent parameters for the three-axle vehicle and six independent parameters for the four-axle vehicle because the sum of w_i equals 1, and there was one redundant parameter. The configuration of the three-axle and the four-axle vehicles are shown in Figs. 7(a and b), respectively.

A qualified fatigue vehicle model should cause almost identical fatigue damage as the load spectrum under considered conditions, including all selected site-specific traffic, a range of span lengths, and different damage locations. The root-mean-square error (RMSE) of FDR was defined as the evaluation function to quantify the errors of fatigue damage calculated by the fatigue vehicle:

$$\mathrm{RMSE}_{\mathrm{FDR}}(s, \boldsymbol{W}, \boldsymbol{L}) = \sqrt{\frac{\sum_{s}\left(\sum_{l=6}^{40}(\mathrm{FDR}(s, l, \mathrm{DL1}, \boldsymbol{W}, \boldsymbol{L}) - 1)^2 + \sum_{l=16}^{40}\sum_{d=\mathrm{DL2}}^{\mathrm{DL3}}(\mathrm{FDR}(s, l, d, \boldsymbol{W}, \boldsymbol{L}) - 1)^2\right)}{\mathrm{num}(s) \times (35 + 25 \times 2)}} \tag{8}$$

where s = selected sites where the fatigue vehicle was used, namely, RD1, RD2,…, RD12; num(s) = number of elements of s; l = single-span length of the bridge; d = fatigue damage location, which could be DL1, DL2, and DL3, shown in Fig. 1; and $\boldsymbol{W}$ and $\boldsymbol{L}$ = axle weight ratio and the axle spacing of the fatigue vehicle, respectively. The FDR could be calculated by s, l, d, $\boldsymbol{W}$, and $\boldsymbol{L}$ by using Eq. (5). The smaller the $\mathrm{RMSE}_{\mathrm{FDR}}$, the higher the accuracy of the fatigue vehicle model to calculate the fatigue damage caused by actual traffic. Therefore, $\boldsymbol{W}$ and $\boldsymbol{L}$ corresponding to the minimal $\mathrm{RMSE}_{\mathrm{FDR}}$ value should be selected as the parameters of the fatigue vehicle.

Since the effects of $\boldsymbol{W}$ and $\boldsymbol{L}$ on $\mathrm{RMSE}_{\mathrm{FDR}}$ are uncertain and irregular, the genetic algorithm (GA) is utilized to identify the minimum value of $\mathrm{RMSE}_{\mathrm{FDR}}$ and the corresponding $\boldsymbol{W}$ and $\boldsymbol{L}$ (Holland 1992). The GA is a mature intelligent algorithm and has been widely applied to various optimization problems (Deng and Cai 2010; Liu et al. 2014b). In this study, the parameter settings of the GA were as follows: the fitness function was set to be the $\mathrm{RMSE}_{\mathrm{FDR}}$; the initial population size = 400; the number of generations = 80; the crossover probability = 0.7; and the mutation probability = 0.01.

It should be noted that since the adjusted Model III represents the best accuracy that could be possibly achieved by the available fatigue vehicle model and the best practice so far, the effectiveness of the proposed fatigue vehicle models in this study will be compared to the accuracy of the adjusted Model III. The goal was that the newly developed fatigue vehicle models could achieve better accuracy and consistence than the adjusted Model III.

First Attempt to Develop a Single Fatigue Vehicle Model

An optimization process of minimizing the $\mathrm{RMSE}_{\mathrm{FDR}}(s_{\mathrm{total}}, \boldsymbol{W}, \boldsymbol{L})$ was carried out to find a single fatigue vehicle model that can be applied to fatigue damage calculations at all 12 sites. According to the research in Zhou et al. (2010), the axle spacing range of the main vehicle types in China was between 1.35 and 7.21 m. Therefore, the constraints of the axle spacing were set between 1.35 and 7.21 m in the optimization process. The optimization mission was set as Eq. (9). Since the initial population of each optimization process was random, the optimization program was run independently and repeatedly several times, and the minimum value of all optimized results was selected as the ultimate result of each vehicle type. Because the optimized $\mathrm{RMSE}_{\mathrm{FDR}}(s_{\mathrm{total}}, \boldsymbol{W}, \boldsymbol{L})$ value of the four-axle fatigue vehicle was smaller than that of the three-axle fatigue vehicle, the four-axle fatigue vehicle was selected as the single fatigue vehicle used for fatigue damage calculations at all 12 sites. The optimized results of $\boldsymbol{W}$ and $\boldsymbol{L}$ of the four-axle vehicle are represented by Eq. (10), and the corresponding FDRs at different sites are presented in Fig. 8

$$\begin{cases} \text{Minimize } \mathrm{RMSE}_{\mathrm{FDR}}(s_{\mathrm{total}}, \boldsymbol{W}, \boldsymbol{L}) \\ \text{subject to} \\ \quad 0 < w_i < 1 \\ \quad \sum w_i = 1 \\ \quad 1.35 < l_i < 7.21 \\ \text{where } s_{\mathrm{total}} = \{\mathrm{RD1},\ \mathrm{RD2},\ \ldots,\ \mathrm{RD12}\} \end{cases} \tag{9}$$

$$\begin{aligned} \boldsymbol{W} &= \{0.14, 0.23, 0.22, 0.41\} \\ \boldsymbol{L} &= \{2.3, 6.0, 3.4\} \end{aligned} \tag{10}$$

The result of $\mathrm{RMSE}_{\mathrm{FDR}}$ of the optimized fatigue vehicle model at 12 selected sites was 0.15, representing an apparent decrease from the value of 0.24 for the adjusted Model III. However, the fatigue damage estimation errors, which was from −52% to 29%, were still too high, especially for short-span bridges under some traffic conditions. Therefore, it can be concluded that the configurations of a fatigue model (including axle weight ratio and axle spacing) have a great influence on the estimated value of fatigue damage, and the accuracy of the fatigue model is able to be modified by adjusting the axle configurations. If a fatigue vehicle model can accurately estimate the fatigue damage by light-duty traffic, then the configurations of the model are close to the characteristics of the light-duty traffic rather than the heavy-duty traffic and then it will produce a large error when calculating the fatigue damage caused by the heavy-duty traffic. Therefore, the optimization process cannot generate a unified model for the fatigue damage estimation under the traffic load of the selected 12 sites; otherwise, it will result in large errors in some cases.

Attempt of Adopting Two Fatigue Vehicles

In this section, a two-model scheme was attempted, which is the result of tradeoff between reducing the number of necessary models for fatigue assessment at 12 sites and improving the accuracy of the models. In order to obtain the two models, a classification of the types of traffic loads was made, and EGVW was chosen as the classification basis because this parameter could reveal the tendency of traffic compositions at different sites. As indicated by the discussions in previous parts, the larger the EGVW, the larger the proportion of six-axle vehicles and the smaller the proportion of two-axle vehicles. Moreover, the EGVW can be directly calculated from the local vehicle weight distribution, which can be easily collected from nearby toll stations.

Based on the previous discussions, the 12 sites are classified into two groups, namely, a light-duty group and a heavy-duty group, according to the EGVW of the site-specific traffic. Sites with an EGVW

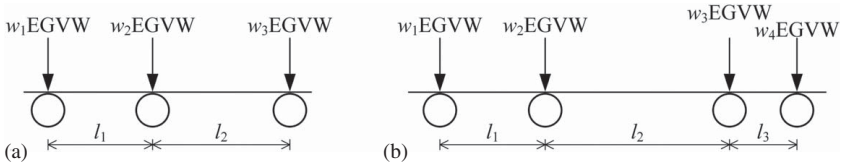

Fig. 7. Axle weights and axle spacings of (a) the three-axle and (b) four-axle fatigue vehicles.

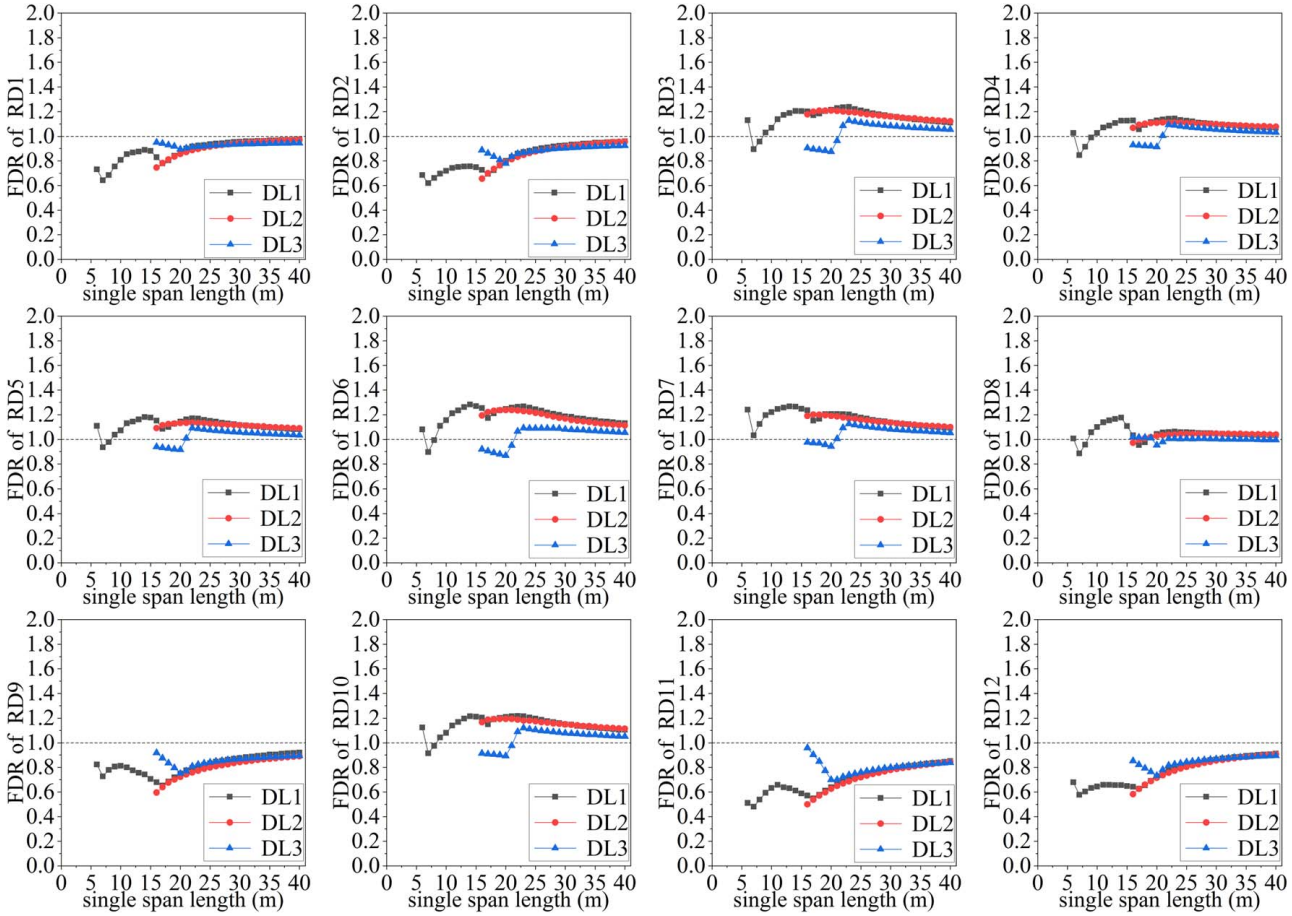

Fig. 8. FDR of the optimized single fatigue vehicle at 12 sites.

less than 300 kN, including RD1, RD2, RD9, RD11, and RD12, are within the light-duty group, while sites with an EGVW greater than 300 kN, namely, RD3, RD4, RD5, RD6, RD7, RD8, and RD10, are assigned to the heavy-duty group. Note that it is assumed in the present research that the fatigue damage caused by the traffic loads of each group can be calculated with the same fatigue vehicle.

In this section, two functions, namely, the $\mathrm{RMSE}_{\mathrm{FDR}}$ of the light-duty group sites and the $\mathrm{RMSE}_{\mathrm{FDR}}$ of the heavy-duty group sites, were defined to quantify the errors of the corresponding fatigue vehicle. It should be stated that the constraints of the axle configuration in this section were the same as the constraints in the previous section. Subsequently, two optimization processes, shown in Eqs. (11) and (12), were carried out individually to search for the minimum values of the two functions.

$$\begin{cases} \text{Minimize } \mathrm{RMSE}_{\mathrm{FDR}}(s_{\mathrm{light}}, \boldsymbol{W}, \boldsymbol{L}) \\ \text{subject to} \\ \qquad 0 < w_i < 1 \\ \qquad \sum w_i = 1 \\ \qquad 1.35 < l_i < 7.21 \\ \text{where } s_{\mathrm{light}} = \{\mathrm{RD1}, \mathrm{RD2}, \mathrm{RD9}, \mathrm{RD11}, \mathrm{RD12}\} \end{cases} \tag{11}$$

$$\begin{cases} \text{Minimize } \mathrm{RMSE}_{\mathrm{FDR}}(s_{\mathrm{heavy}}, \boldsymbol{W}, \boldsymbol{L}) \\ \text{subject to} \\ \qquad 0 < w_i < 1 \\ \qquad \sum w_i = 1 \\ \qquad 1.35 < l_i < 7.21 \\ \text{where } s_{\mathrm{heavy}} = \{\mathrm{RD3}, \mathrm{RD4}, \mathrm{RD5}, \mathrm{RD6}, \mathrm{RD7}, \mathrm{RD8}, \mathrm{RD10}\} \end{cases} \tag{12}$$

The two optimization processes of Eqs. (11) and (12) were conducted utilizing the GA, similar to the process of the first attempt to develop the single-vehicle model in the previous section. The parameter settings of the GA were described in the previous section. Each optimization process was carried out several times randomly to obtain the minimum value of $\mathrm{RMSE}_{\mathrm{FDR}}$, both for the three-axle fatigue vehicle form and the four-axle fatigue vehicle form.

The optimized $\mathrm{RMSE}_{\mathrm{FDR}}$ value of the four-axle vehicle was less than that of the three-axle vehicle in both the light-duty and heavy-duty traffic groups. However, the spacing of the two rear axles was too short, but the weight difference between the two rear axles was significantly large for the optimized four-axle vehicle in the light-duty traffic group, which is abnormal for a vehicle model. Therefore, the optimized three-axle vehicle was selected for the light-duty group, and the optimized four-axle vehicle was selected for the heavy-duty group. The optimization results of the two fatigue vehicles are shown in Fig. 9. The FDR values of the newly proposed two vehicles are expressed in Figs. 10 and 11. In addition, the $\mathrm{RMSE}_{\mathrm{FDR}}$ values of fatigue vehicles under different traffic groups are shown in Table 3.

It can be observed by comparing Fig. 10 with Fig. 6 that the accuracy of the fatigue damage calculated with the newly proposed light-duty fatigue vehicle is apparently improved compared with that calculated with the adjusted Model III, especially for short-span bridges with a single span length ranging from 6 to 23 m. Specifically, for simply supported girder bridges with a single span length ranging from 6 to 23 m in RD12, the fatigue estimation errors calculated by the adjusted Model III at DL1 varied from −54% to 1%, while the errors calculated by the newly proposed light-duty

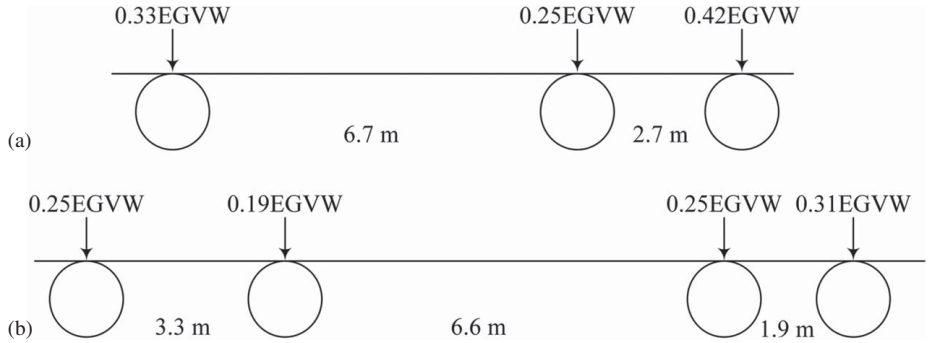

Fig. 9. Axle configuration of (a) light-duty fatigue vehicle; and (b) heavy-duty fatigue vehicle.

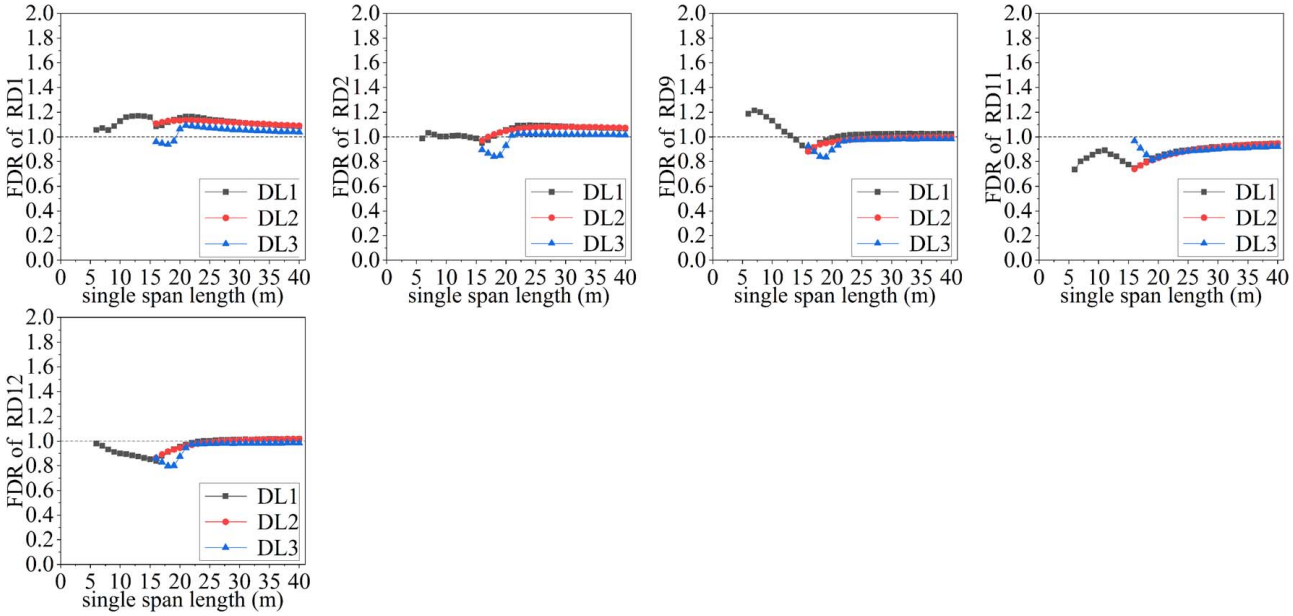

Fig. 10. FDR of the light-duty fatigue vehicle.

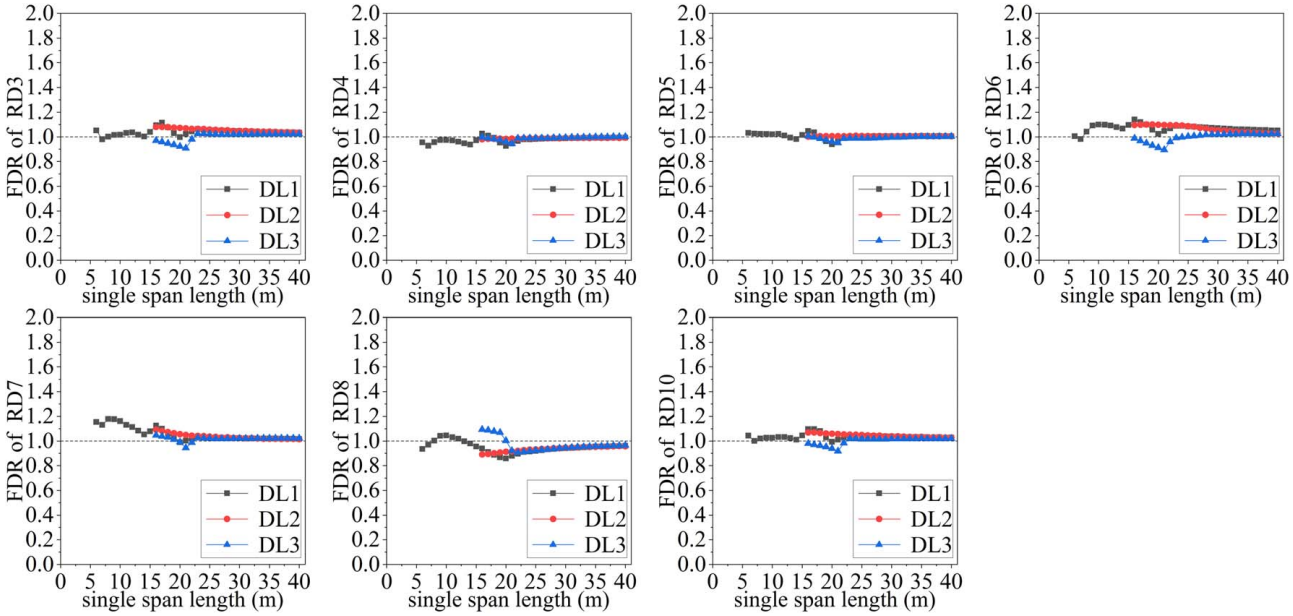

Fig. 11. FDR of the heavy-duty fatigue vehicle.

Table 3. $RMSE_{FDR}$ of fatigue vehicles under different traffic conditions

Fatigue vehicle	Light-duty traffic	Heavy-duty traffic
Model III	0.16	0.31
Light-duty fatigue vehicle	0.09	—
Heavy-duty fatigue vehicle	—	0.05

fatigue vehicle varied within a much smaller range of −16% to −1%. When the bridge span increased to larger than 23 m, the errors calculated by the newly proposed light-duty fatigue vehicle were still smaller, although the errors calculated by the two models both gradually decreased. Overall, for the traffic loads in the five sites of the light-duty group, the FDR of the new light-duty fatigue vehicle under all considered span lengths and damage locations ranged from 0.74 to 1.21, and the corresponding relative errors were from −26% to 21%. Compared with the relative error range of the adjusted Model III from −54% to 23%, the upper and lower bounds of the relative errors of the new light-duty fatigue vehicle were obviously reduced in calculating the fatigue damage at light-duty sites. In addition, for the new light-duty fatigue vehicle, the $RMSE_{FDR}$ at the light-duty sites was sharply reduced from 0.16 of the adjusted Model III to 0.09, which indicates that the accuracy of the newly proposed light-duty fatigue vehicle is greatly improved.

Similar conclusions could also be made for the newly proposed heavy-duty fatigue vehicle. By comparing Fig. 11 with Fig. 6, it can be found that the accuracy of the fatigue damage calculated with the newly proposed heavy-duty fatigue vehicle is dramatically improved compared with that calculated with the adjusted Model III under all considered span lengths. Specifically, for girder bridges in RD10, the fatigue estimation errors calculated with the adjusted Model III at DL1 and DL3 ranged from −17% to 67% and from −28% to 39%, respectively, while the errors calculated with the newly proposed heavy-duty fatigue vehicle just ranged from −1% to 10% and from −8% to 2%, respectively. Overall, for the traffic loads in the seven sites of the heavy-duty group, the FDR of the heavy-duty fatigue vehicle under all considered span lengths and damage locations ranged from 0.86 to 1.18, which means that the corresponding relative errors ranged from −14% to 18%. Compared with the error range of the adjusted Model III from −29% to 84%, the error range of the new heavy-duty fatigue vehicle was significantly reduced. Moreover, the $RMSE_{FDR}$ under all selected conditions in the heavy-duty group was sharply reduced from 0.31 for the adjusted Model III to 0.05 for the new heavy-duty fatigue vehicle.

In summary, based on the analysis of the FDR of different fatigue vehicles under different conditions, it was found that compared with results with the adjusted Model III, the accuracy of the newly proposed two models, namely, the light-duty fatigue vehicle and the heavy-duty fatigue vehicle, was highly improved in calculating the vehicle-induced fatigue damage under considered conditions. In particular, for the heavy-duty fatigue vehicle, the $RMSE_{FDR}$ under the selected heavy-duty traffic was sharply reduced from 0.31 to 0.05, which showed that the accuracy of the new model was greatly improved in heavy-duty traffic compared to the adjusted Model III. Moreover, the results showed that classifying traffic before the optimization process was helpful for proposing new fatigue vehicles with improved accuracy. Furthermore, the EGVW could be an effective indicator to make this classification.

Summary and Conclusions

In this study, a new method for developing fatigue vehicle models applicable to various sites with different traffic conditions is proposed. The traffic in China is used as the background and the collected vehicle load spectra from 12 typical sites are used as an example to illustrate the procedure of the method. A two-vehicle-model scheme, i.e., a three-axle vehicle model and a four-axle vehicle model that represent the light-duty traffic and heavy-duty traffic, respectively, is proposed. Based on the results from the present study, the following conclusions can be drawn:

(1) The vehicle load spectra and the equivalent gross vehicle weights depend strongly on the site locations. The relation between the frequency of occurrence of each vehicle type and the percentage of fatigue damage caused by that type of vehicle is not straightforward. In some areas, the largest proportion of fatigue damage may be caused by heavy vehicles with a small frequency of occurrence.
(2) The accuracy of Model III in the Chinese specification is related to both the site-specific traffic load compositions and the damage locations and span lengths of bridges. The relative errors of the fatigue damage calculated with Model III can be very large for some regions. By adopting an adjusted Model III with the gross vehicle weight adjusted to the site-specific EGVW, the errors can be significantly reduced. Yet, due to the inherent limitation with the single fatigue vehicle model, the errors are still within a relatively large range.
(3) Both the axle weight ratio and axle spacing of fatigue vehicles have strong effects on the accuracy of the fatigue damage calculation. A single fatigue vehicle model is obtained for all the 12 sites considered in the present research by using an optimization method in the first attempt. It is found that the single fatigue vehicle model has improved accuracy over the adjusted Model III but still give results with errors greater than 30% when simply used for the fatigue damage calculation due to the differences in traffic load compositions at different sites.
(4) The proposed two-vehicle-model scheme that includes a three-axle vehicle and a four-axle vehicle was found to be more accurate and consistent than a single model scheme for various traffic load compositions. In particular, the root-mean-square error of the estimated fatigue damage at sites with heavy traffic is within 5% when using the developed four-axle fatigue vehicle, which is significantly lower than that of the adjusted Model III.

In summary, the proposed method in this study provides a good approach for developing fatigue vehicle models for regions where the traffic load composition may vary significantly between different sites. In addition, the fatigue vehicle models developed in the present study can be used as a reference for the calculation of vehicle-induced bridge fatigue damage in China.

Data Availability Statement

Some data, models, or code generated or used during the study are available from the corresponding author by request, including the traffic data and the algorithm used to develop the fatigue vehicle model.

Acknowledgments

The authors would like to acknowledge the financial support provided by the National Natural Science Foundation of China (Grant Nos. 51808209 and 51778222), the Natural Science Foundation of Hunan Province (2019JJ50065), and the Fundamental Research Funds for the Central Universities (Grant No. 531118010081).

References

AASHTO. 2017. *LRFD bridge design specifications*. Washington, DC: AASHTO.

Brühwiler, E., and A. Herwig. 2008. "Consideration of dynamic traffic action effects on existing bridges at ultimate limit state." In *Proc., 4th Int. Conf. on Bridge Maintenance, Safety, Management, Health Monitoring and Informatics*, 712–713. London, UK: Taylor & Francis.

CEN (European Committee for Standardization). 2003. *Eurocode 1: Action on structures-Part 2: Traffic loads on bridges*. Brussels, Belgium: CEN.

Chen, W. Z., J. Xu, B. C. Yan, and Z. P. Wang. 2015. "Fatigue load model for highway bridges in heavily loaded areas of China." *Adv. Steel Constr.* 11 (3): 322–333.

Chotickai, P., and M. D. Bowman. 2006. "Truck models for improved fatigue life predictions of steel bridges." *J. Bridge Eng.* 11 (1): 71–80. https://doi.org/10.1061/(ASCE)1084-0702(2006)11:1(71).

Croce, P. 2001. "Background to fatigue load models for Eurocode 1: Part 2 traffic loads." *Prog. Struct. Mater. Eng.* 3 (4): 335–345. https://doi.org/10.1002/pse.93.

Deng, L., and C. S. Cai. 2010. "Bridge model updating using response surface method and genetic algorithm." *J. Bridge Eng.* 15 (5): 553–564. https://doi.org/10.1061/(ASCE)BE.1943-5592.0000092.

Deng, L., W. Wang, and X. H. He. 2017. "Optimization and application of fatigue design based on AASHTO code." *China J. Highway Transport* 30 (3): 40–48.

Deng, L., and W. Yan. 2018. "Vehicle weight limits and overload permit checking considering the cumulative fatigue damage of bridges." *J. Bridge Eng.* 23 (7): 04018045. https://doi.org/10.1061/(ASCE)BE.1943-5592.0001267.

Downing, S. D., and D. F. Socie. 1982. "Simple rainflow counting algorithms." *Int. J. Fatigue* 4 (1): 31–40. https://doi.org/10.1016/0142-1123(82)90018-4.

GB (Guobiao Standard). 2015a. *General specifications for design of highway bridges and culverts*. JTG D60-2015. Beijing: China's Ministry of Transport.

GB (Guobiao Standard). 2015b. *Specifications for design of highway steel bridge*. JTG D64-2015. Beijing: China's Ministry of Transport.

González, A., D. Cantero, and E. J. OBrien. 2011. "Dynamic increment for shear force due to heavy vehicles crossing a highway bridge." *Comput. Struct.* 89 (23–24): 2261–2272. https://doi.org/10.1016/j.compstruc.2011.08.009.

Han, Y., K. Li, C. S. Cai, L. Wang, and G. Xu. 2020. "Fatigue reliability assessment of long-span steel-truss suspension bridges under the combined action of random traffic and wind loads." *J. Bridge Eng.* 25 (3): 04020003. https://doi.org/10.1061/(ASCE)BE.1943-5592.0001525.

Holland, J. H. 1992. *Adaptation in natural and artificial systems: An introductory analysis with applications to biology, control, and artificial intelligence*. Cambridge, MA: MIT Press.

Laman, J. A., and A. S. Nowak. 1996. "Fatigue-load models for girder bridges." *J. Struct. Eng.* 122 (7): 726–733. https://doi.org/10.1061/(ASCE)0733-9445(1996)122:7(726).

Liu, G., Z. Wei, and Y. Yang. 2014a. "Research on vehicular loads and fatigue load model of urban road bridge." [In Chinese.] *J. Highway Transp. Res. Dev.* 31 (6): 86–93.

Liu, M. 2017. "Research on fatigue load spectrum of expressway bridge vehicles based on WIM." [In Chinese.] *Highways Automot. Appl.* 3: 152–155.

Liu, S., Q. Yan, J. Yang, and X. Zhao. 2017a. "Research on fatigue load model of heavy traffic highway bridges in Fujian Province." [In Chinese.] *Fujian Transp. Technol.* 4: 119–122.

Liu, Y., D. Li, Z. Zhang, H. Zhang, and N. Jiang. 2017b. "Fatigue load model using the weigh-in-motion system for highway bridges in China." *J. Bridge Eng.* 22 (6): 04017011. https://doi.org/10.1061/(ASCE)BE.1943-5592.0001048.

Liu, Y., N. Lu, M. Noori, and X. Yin. 2014b. "System reliability-based optimisation for truss structures using genetic algorithm and neural network." *Int. J. Reliab. Saf.* 8 (1): 51–69. https://doi.org/10.1504/IJRS.2014.062640.

Lu, N., M. Noori, and Y. Liu. 2017. "Fatigue reliability assessment of welded steel bridge decks under stochastic truck loads via machine learning." *J. Bridge Eng.* 22 (1): 04016105. https://doi.org/10.1061/(ASCE)BE.1943-5592.0000982.

Ma, R., S. Xu, D. Wang, and A. Chen. 2018. "Vehicle models for fatigue loading on steel box-girder bridges based on weigh-in-motion data." *Struct. Infrastruct. Eng.* 14 (6): 701–713. https://doi.org/10.1080/15732479.2017.1359308.

Miner, M. A. 1945. "Cumulative fatigue damage." *J. Appl. Mech.* 12 (3): A159–A164.

Qin, S., and Z. Gao. 2017. "Developments and prospects of long-span high-speed railway bridge technologies in China." *Engineering* 3 (6): 787–794.

Raju, S. K., F. Moses, and C. G. Schilling. 1990. "Reliability calibration of fatigue evaluation and design procedures." *J. Struct. Eng.* 116 (5): 1356–1369. https://doi.org/10.1061/(ASCE)0733-9445(1990)116:5(1356).

Schilling, C. G. 1984. "Stress cycles for fatigue design of steel bridges." *J. Struct. Eng.* 110 (6): 1222–1234. https://doi.org/10.1061/(ASCE)0733-9445(1984)110:6(1222).

Schilling, C. G., and K. H. Klippstein. 1977. "Fatigue of steel beams by simulated bridge traffic." *J. Struct. Div.* 103 (8): 1561–1575.

Sedlacek, G., G. Merzenich, M. Paschen, A. Bruls, L. Sanpaolesi, P. Croce, M. Pratt, M. Leendertzet al.. 2008. *Background document to EN 1991-Part 2-Traffic loads for road bridges-and consequences for the design*. JRC Scientific Technical Report. Brussels, Belgium: European Commission.

Shao, Y., and P. Lu. 2015. "Fatigue load spectrum for Jiujiang Yangtze River Bridge." [In Chinese.] *J. Chang'an Univ. (Nat. Sci. Ed.)* 35 (5): 50–57.

Su, J., G. Zhou, and N. Wang. 2018. "Research on vehicle model of fatigue load of Jiqing expressway bridge." [In Chinese.] *J. Highway Transp. Res. Dev.* (5): 6.

Sun, S., and L. Sun. 2012. "Statistic model of vehicle loads for highway bridges." [In Chinese.] *J. Tongji Univ.* 40 (2): 198–204.

Tong, L., Z. Shen, and Z. Chen. 1997. "Fatigue load spectrum of urban road bridges." [In Chinese.] *China Civ. Eng. J.* 30 (5): 20–27.

Yan, B. C., W. Z. Chen, and J. Xu. 2012. "Analysis of the current situation of highway traffic load in China." In *Proc., 1st Int. Conf. on Performance-Based and Life-Cycle Structural Engineering*, 1278–1286. Hong Kong, China: Hong Kong Polytechnic University.

Yang, Z. 2015. *Research on load model of actual operating vehicles on typical highway*. [In Chinese.] Nanjing, China: Southeast Univ.

Yin, X. 2016. *Prediction of overweight vehicles and research on standard fatigue vehicle load in middle and late industrialized regions*. [In Chinese.] Guangzhou, China: Guangzhou Univ.

Zhao, J. 2014. *Research on normal vehicle load and extra-heavy truck load of multi-regional highway bridges*. [In Chinese.] Shaanxi, China: Chang'an Univ.

Zhou, X., and X. Zhang. 2019. "Thoughts on the development of bridge technology in China." *Engineering* 5 (6): 1120–1130.

Zhou, Y., W. Bao, H. Zhai, and Y. Liu. 2010. "Study of standard fatigue design load for steel highway bridges." [In Chinese.] *China Civ. Eng. J.* 43 (11): 79–85.

Zhou, Y., H. Zhai, W. Bao, and Y. Liu. 2009. "Research on standard fatigue vehicular load for highway bridges." [In Chinese.] *Highway* 12: 21–25.